

Co-published by Institute of Fluid-Flow Machinery Polish Academy of Sciences

Committee on Thermodynamics and Combustion

Polish Academy of Sciences

Copyright©2025 by the Authors under licence CC BY-NC-ND 4.0

http://www.imp.gda.pl/archives-of-thermodynamics/



Sensitivity Analysis of Magnetohydrodynamic Mixed Convective Trapezoidal Heat Exchanger Containing Hybrid Nanofluid: Numerical and Statistical Approach

Saiful Islam^a, Goni Molla^b, Badhan Neogi^a, Muhammad Faiaz^a, B.M. Jewel Rana^c, Md. Mamun Molla^{d,e*}

^aDepartment of Mathematics, Gopalganj Science and Technology University, Gopalganj 8100, Bangladesh
^bDepartment of Applied Physics, Electronics & Communication Engineering, Gopalganj Science and Technology University, Gopalganj 8100, Bangladesh
^cDepartment of Quantitative Sciences (Mathematics), International University of Business Agriculture and Technology, Dhaka 1230, Bangladesh
^dDepartment of Mathematics & Physics, North South University, Dhaka 1229, Bangladesh
^eCenter for Applied and Computational Sciences (CACS), North South University, Dhaka 1229, Bangladesh
*Corresponding author email: mamun.molla@northsouth.edu

Received: 02.09.2024; revised: 02.05.2025; accepted: 05.05.2025

Abstract

The consequences of magnetohydrodynamic mixed convection in a trapezoidal heat exchanger are investigated through numerical analysis. Due to the extensive applications of both mono and hybrid nanofluids in manufacturing and thermal engineering, the Ag-MgO-H₂O hybrid nanofluid is selected as the working material for the entire domain. Additionally, a horizontal magnetic field is applied to the cavity. The finite element method is involved to solve the corresponding mathematical equations. The physical implications of the results are examined over a range of Reynolds numbers ($10 \le \text{Re} \le 200$), Hartmann numbers ($0 \le \text{Ha} \le 100$), and nanoparticle volume fractions ($0 \le \phi \le 0.08$) using streamlines, isotherms, and line graphs. The impact of key factors on the response function is illustrated using the response surface methodology with 2D and 3D visualizations. Sensitivity rates are analysed by developing a best-fit correlation. It is concluded that the thermal enhancement of the hybrid nanofluid is achieved up to 11.4% by incorporating hybrid nanoparticles, and due to the upsurge of the Reynolds number. Conversely, the influence of the magnetic field leads to a decline in this rate to 10.02%. The use of Ag-MgO-H₂O hybrid nanofluid improves the heat transfer efficiency of water by 6.62%. Finally, the results of this study may offer valuable insights for designing an efficient mixed convective mechanical device.

Keywords: Hybrid nanofluid; Mixed convection; Heat exchanger; Response surface methodology; Sensitivity analysis

Vol. 46(2025), No. 3, 61-76; doi: 10.24425/ather.2025.156579

Cite this manuscript as: Islam, S., Molla, G., Neogi, B., Faiaz, M., Rana, B.M.J., & Molla, M.M. (2025). Sensitivity Analysis of Magneto-hydrodynamic Mixed Convective Trapezoidal Heat Exchanger Containing Hybrid Nanofluid: Numerical and Statistical Approach. *Archives of Thermodynamics*, 46(3), 61–76.

1. Introduction

Current researchers are also captivated by mixed convective heat transfer involving fluid movement in enclosed spaces, where the combination of forced and natural convection results in mixed convection. This phenomenon has gained increasing attention in metallworking and metallurgical sciences due to its substantial influence on the heat transfer of electrically conductive fluids. The investigation, understanding, and prediction of fluid flow dynamics have been of great interest. Leonardo da Vinci was the first to observe and document fluid flow phenomena in the early fifteenth century, sparking a substantial amount of research in fluid mechanics. Mixed convective heat transfer in various enclosures is a crucial topic in engineering sectors because of its extensive applications in heat exchangers, nuclear reactors, drying technologies, solar panels, building in-

Nomenclature

 c_p – specific heat at constant pressure, J/(kg·K)

Ha - Hartman number

Nu - Nusselt number

p - pressure, kPa

P – dimensionless pressure

Pr -Prandtl number

Re - Reynolds number

Ri - Richardson number

T - temperature, K

u, v-dimensional velocity, m/s

U, V- dimensionless velocity

Greek symbols

α – thermal diffusivity, m²/s²

β – coefficient of thermal expansion, K⁻¹

 θ – dimensionless temperature

 μ – dynamic viscosity, kg/(m·s)

v – kinematic viscosity, m²/s

 ρ – density, kg/m³

 σ – electric conductivity, $\Omega^{-1} \cdot m^{-1}$

 ϕ – particle concentration

 ψ – stream function

 Ω – vorticity vector

Subscripts and Superscripts

HS - hot surface

hnf – hybrid nanofluid

Abbreviations and Acronyms

FEM - finite element method

RSM - response surface methodology

sulation, lubrication technologies, and chemical industries. Among the most studied areas are mixed convective flows in enclosed spaces, aiming for a quantitative understanding and expanding their practical applications [1-5]. Nanofluids, which consist of nanoparticles with diameters less than 100 nm, enhance the thermodynamic properties and thermal efficiency of base fluids even at low concentrations when properly dispersed and stabilised [6–10]. Numerous researchers have explored methods to improve heat transfer and cooling effects by considering various geometries and configurations of different nanofluids [11–15]. In the context of a variety of engineering and industrial applications for nanofluids, it is essential to significantly modify the attributes of mono nanofluids significantly to enhance their thermophysical and rheological properties. To meet these needs, a new type of fluids known as hybrid nanofluids (HNFs) were developed. These fluids allow for the proper combination of two or more nanoparticles within a single base fluid. Essentially, composite or hybrid nanofluids are a novel category of nanofluids created by mixing metal oxide, metal particles, or both into a primary fluid. Significant research has already been conducted on hybrid nanofluids. For instance, Kaushik et al. [16] conducted both numerical and experimental studies to compare the flow behaviour between CuO-ZnO-H2O and the base fluid in a small channel. They concluded that due to the addition of solid nanoparticles, the outcomes improved up to 18-21%. Hussain et al. [17] used numerical methods to study an open enclosure with a square adiabatic barrier, using Al₂O₃-Cu-H₂O hybrid nanofluid. Their findings indicated that the rate of heat transfer was enriched by increasing the Richardson number, Reynolds number, and nanoparticle size. Zaboli et al. [18] reported that hybrid nanofluids could enhance heat exchange in solar systems, including trough collectors. Mahalakshmi [19] conducted a numerical study on a lid-driven mixed convection with heat sources containing hybrid nanofluids. The study concluded that the Ag-CuO-water hybrid nanofluid transfers heat more efficiently compared to Ag-MgO-water and Ag-TiO2-water. Mandal et al. [20] numerically explored the effects of several geometric factors on a porous W-shaped cavity experie-ncing mixed convection with a Cu-Al₂O₃-H₂O hybrid nanofluid. They found that increasing the bottom undulation amplitude im-

proved thermal energy transmission despite the reduced fluid volume. Anee et al. [21] applied the Lattice Boltzmann method (LBM) to examine the heat transfer behaviour of hybrid nanofluid in an enclosed shape with multiple heaters, revealing that the size of the nanoparticles and the Hartmann number (Ha) significantly affected heat transfer. Thumma et al. [22] studied the heat transfer phenomena of a magnetised hybrid nanofluid (Cu-Ag-H₂O) in a radiative flow across a rotating disc, taking into account the Hall current and heat source. Their investigation showed that the Hall current parameter not only regulates crossradial velocity and energy but also increases radial motion. The hybrid nanofluid exhibited superior heat transfer performance compared to a single fluid with respect to thermal radiation and ESHS coefficients.

The study of the influence of magnetic forces on electrically conducting fluids is known as magnetohydrodynamics (MHD). MHD encompasses mechanisms such as the Earth's magnetic field, nuclear fusion, cooling of fission reactors, X-ray radiation, and solar wind cooling. Various researchers have examined MHD heat transfer in different enclosures over time due to these practical applications [23-27]. Owing to its numerous uses, MHD mixed convection involving various geometries, temperatures, and boundary conditions has garnered significant attention in scientific research. For instance, Tayebi et al. [28] explored heat transfer behaviour of a hybrid nanofluid in a square cavity including a wavy cylinder. Gibanov et al. [29] investigated MHD of ferrofluid in a chamber with moving upper edges and a porous layer. Mebarek-Oudina et al. [30] studied the magnetohydrodynamic transport of a hybrid nanofluid within a porous chamber, finding that the upsurge of magnetic field intensity inhibits the convective heat transfer rate. Selimefendigil and Chamkha [31] completed a numerical study on MHD flow in a square cavity with a partial triangular porous layer, filled with Ag-MgO-water hybrid nanofluid. They observed that increasing the porosity of the container significantly boosts heat transfer, while the presence of a magnetic field substantially decreases it. Ma et al. [32] statistically examined the MHD effects using a Shamse Knot-shaped cavity filled with Ag-TiO2-water hybrid nanofluid, discovering that MHD influences heat transfer and that increases in the Rayleigh number (Ra) and cavity side

length (D) enhance heat transport. Munawar et al. [33] numerically studied MHD mixed convection using Ag-MgO-water in an inclined cavity with a circular heater. They determined that increasing the Hartmann number (Ha) reduces the average Nusselt number (Nu_{av}), and greater heat transfer rates were achieved by using central heaters with smaller radii for free convection and larger radii for forced convection. Mourad et al. [34] explored the impact of MHD on a hybrid nanofluid within a wavy cavity using the finite element method (FEM). Their findings indicated that Nu_{av} increases with the Darcy number (Da) and Ra but decreases with Ha.

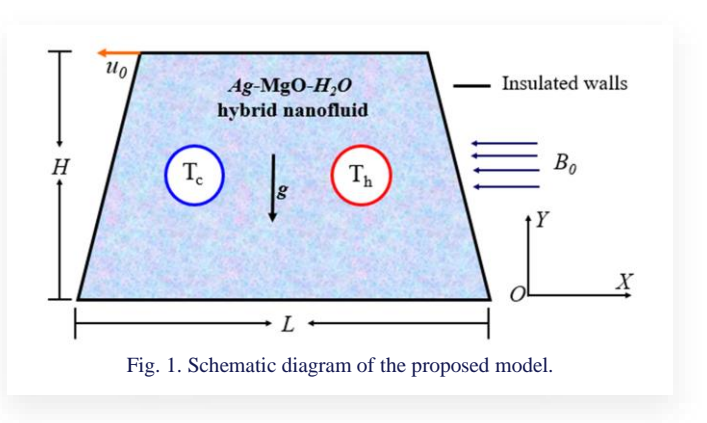
An apparatus that moves heat from an energy source to a working fluid is called a heat exchanger. It is utilised in systems that heat and cool, where the fluids may be near one another or kept apart by a solid barrier to avoid direct contact. Heat exchangers are essential in different applications, such as ventilation, freezing, sewage treatment, chemical and pharmaceutical plants, power plants, natural gas processing, and space heating [35–39]. Chen et al. [40] developed a heat exchanger model to explore the relationship between fin pitches and tube diameters in a fintube heat exchanger, using both numerical and experimental methods to solve it. Lee et al. [41] created a 3D model of unsteady free convection for a circular fin-tube heat exchanger. Additionally, Pakalka et al. [42] developed a theoretical and experimental framework for a heat exchanger based on fin-tube design.

The review of publications mentioned above makes it evident that the MHD mixed convective heat exchanger is a subject of great attraction to investigators on account of its creative uses across a wide range of engineering sectors. While numerous studies have been conducted on a variety of cavities to examine mixed convective fluid with MHD and heat transfer mechanisms, some recent studies have focused on schematic cavities that can hold a wide variety of nanoparticles [43–46]. Similarly, comparatively little research was done on heat exchangers to construct a fast heat transmission structure [47–49]. Yet, in the current research, a sensitivity analysis of a trapezoidal heat exchanger that contains an Ag-MgO-H₂O hybrid nanofluid using RSM is performed after integrating these two phenomena, heat exchanger and mixed convection. Moreover, in rela life aplications, there are numerous trapezoildal-shaped industrial architecture where mono or hybrid nanofluids are used for distinct purposes. To the greatest of the writer's understanding, no investigation has been done on this topic yet. The FEM is a popular computational technique that is used to simulate the governing formulas [50, 51]. Another reason to implement the RSM is to investigate the geometric and statistical impact of involved parameters with a best-fitted correlation with Nuav and involved parameters. Investigating the heat transfer mechanisms for this hybrid nanofluid-based mixed convective trapezoidal heat exchanger mathematically and statistically using FEM and RSM is the primary goal of this study.

2. Physical description and mathematical model

Using water (H₂O) as the primary fluid, a schematic-shaped cavity is examined numerically as a fluid region containing Ag and MgO nanoparticles. This fluid is an incompressible, steady and

Newtonian fluid that takes magnetic field impacts into ac-count. The height and length of this schematic-shaped cavity, which is mass and heat isolated, are H and L, accordingly. With a lid motion of u, the top horizontal wall is moving. On the right and left sides, accordingly, two cylinder pipes with a 0.1L radius can be utilized as a heater and cooler. Figure 1 shows the ar-rangement of this fluid framework with a schematic-shaped heat exchanger. It is proposed that the left cylindrical pipe indicates a cool surface T_c while the right pipe indicates a hot surface T_h .



The outer boundaries of the fluid area are totally intact and adiabatic. Additionally, the gravitational acceleration g works in the exact reverse position of the Y-dimension. Further, the frame is enveloped by a B_0 form of Ag-MgO magnetic field that is constant and flows from right to left. The nearby medium is considered non-slip because of the assumed equality of size and nanoparticles. In this situation, Table 1 lists the thermophysical properties of the considered nanofluid.

Table 1. Characteristics of nanoparticles and base fluid [52].

Nanoparticle and base fluid	c_p , J·kg ⁻¹ ·K ⁻¹	ρ, kg·m ⁻³	<i>κ</i> , W·m⁻¹·K⁻¹	<i>β</i> , K ⁻¹	<i>σ</i> , S·m ⁻¹	μ, kg·m ⁻¹ ·s ⁻¹
Ag	235	10500	429	5.4×10 ⁻⁵	8.1×10 ⁻⁴	-
MgO	879	3970	30	3.36×10 ⁻⁵	8×10 ⁻⁴	-
H ₂ O	4179	997.1	0.613	21×10 ⁻⁵	5.5×10 ⁻⁶	8.91×10 ⁻⁴

Some assumptions served as the foundation for this study and the creation of the model. The following assumptions were considered:

- (i) this hybrid nanofluid has a two-dimensional laminar, incompressible flow,
- (ii) magnetohydrodynamic mixed convection is considered,
- (iii) the governing equations are simulated using the Galerkin weighted residual finite element method,
- (iv) the flow problem is considered under the Boussinesq approximation.

To see the entire fluid flow area, a two-dimensional (2D) Cartesian structure is set up, with the left sidewall marked by the *Y*-axis and the bottom wall by the *X*-axis. The basic governing equations to make a mathematical form for this mixed convective two dimensional model using hybrid nanofluid are the continuity, momentum, and energy equations as follows:

$$\frac{\partial u}{\partial x} + \frac{\partial v}{\partial y} = 0,\tag{1}$$

Islam S., Molla G., Neogi B., Faiaz M., Rana B.M.J., Molla M.M.

$$\rho_{hnf}\left(\frac{\partial u}{\partial x} + \frac{\partial u}{\partial y}\right) = -\frac{\partial p}{\partial x} + \mu_{hnf}\left(\frac{\partial^2 u}{\partial x^2} + \frac{\partial^2 u}{\partial y^2}\right) + F, \quad (2a)$$

$$\rho_{hnf}\left(\frac{\partial v}{\partial x} + \frac{\partial v}{\partial y}\right) = -\frac{\partial p}{\partial y} + \mu_{hnf}\left(\frac{\partial^2 v}{\partial x^2} + \frac{\partial^2 v}{\partial y^2}\right) + F, \quad (2b)$$

$$\frac{\partial T}{\partial x} + \frac{\partial T}{\partial y} = \frac{k_{hnf}}{(\rho c_p)_{hnf}} \left(\frac{\partial^2 T}{\partial x^2} + \frac{\partial^2 T}{\partial y^2} \right). \tag{3}$$

Here, in the *u*-momentum equation, there is no external effect; as a result, Eq. (2a) does not include any additional body force (F=0); Eq. (2b) adds $F = g(\rho\beta)_{hnf}(T - T_c) - \mu_{hnf}B_0^2v$ because of an outside magnetic field and gravitational force. Also, the dimensionless initial and boundary conditions are:

At right circular surface:
$$T=T_h$$
, $u=v=0$ At left circular surface: $T=T_c$, $u=v=0$ Rest of the walls: $\frac{\partial T}{\partial n}=0$, $u=v=0$

Additionally, Table 2 explains the correlations of hybrid nanofluids which have been taken into account between base fluid (H₂O) and nanoparticles (Ag and MgO). Here, *n* is the orthogonal unit vector on the *XY*-plane. To put it practically, base fluid and nanoparticles are needed to obtain the properties of nanofluid. The correlations that are taken into consideration between primary fluid (H₂O) and nanoparticles (Ag and MgO) are explained in this part of the paper. The characteristics of nanofluid are truly dependent upon the primary fluid and nanomaterials. In order to estimate the characteristics of nanofluids, correlations gathered in Table 2 are used.

Table 2. Used correlations of hybrid nanofluid [53].

Properties	Applied Correlations
Concentration of nanoparticles	$\phi = \phi_{Ag} + \phi_{MgO}$
Density of nanofluid	$ ho_{hnf}=(1-\phi) ho_{bf}+\phi ho_{sp}$ where: $\phi ho_{sp}=\phi_{ m Ag}\phi ho_{ m Ag}+\phi_{ m MgO} ho_{ m MgO}$
Specific heat capacity	$egin{aligned} \left(ho c_p ight)_{hnf} &= (1-\phi) \left(ho c_p ight)_{bf} + \phi \left(ho c_p ight)_{sp} \ \end{aligned}$ where: $\phi \left(ho c_p ight)_{sp} = \phi_{ m Ag} \left(ho c_p ight)_{ m Ag} + \phi_{ m MgO} \left(ho c_p ight)_{ m MgO}$
Thermal conductivity	$\kappa_{hnf} = \kappa_{bf} \left\{ \frac{\kappa_{sp} + 2\kappa_{bf} - 2\phi(\kappa_{bf} - \kappa_{sp})}{\kappa_{sp} + 2\kappa_{bf} + \phi(\kappa_{bf} - \kappa_{sp})} \right\}$ where: $\phi \kappa_{sp} = \phi_{Ag} \kappa_{Ag} + \phi_{MgO} \kappa_{MgO}$
Thermal diffusivity	$\alpha_{hnf} = \frac{k_{hnf}}{\left(\rho c_p\right)_{hnf}}$
Dynamic viscosity	$\mu_{hnf} = \mu_{hnf} (1 + 2.5\phi + 6.2\phi^2)$
Thermal expansion coefficient	$(hoeta)_{hnf} = (1-\phi)(hoeta)_{bf} + \phi(hoeta)_{sp}$ where: $\phi(hoeta)_{sp} = \phi_{\mathrm{Ag}}(hoeta)_{\mathrm{Ag}} + \phi_{\mathrm{MgO}}(hoeta)_{\mathrm{MgO}}$
Electrical conductivity	$\sigma_{hnf} = \sigma_{bf} \left[1 + \frac{3\phi \left(\frac{\sigma_{sp}}{\sigma_{bf}} - 1 \right)}{\left(\frac{\sigma_{sp}}{\sigma_{bf}} + 2 \right) - \phi \left(\frac{\sigma_{sp}}{\sigma_{bf}} - 1 \right)} \right]$ where: $\phi \sigma_{sp} = \phi_{Ag} \sigma_{Ag} + \phi_{MgO} \sigma_{MgO}$

By incorporating the dimensionless quantities in Eq. (5) into Eqs. (1–3), the subsequent dimensionless governing equations (6–9) are generated:

$$X = \frac{x}{L}, \qquad Y = \frac{y}{L}, \qquad U = \frac{u}{u_0},$$

$$V = \frac{v}{u_0}, \qquad P = \frac{p}{\rho_{nf}u_0^2} \quad \text{and} \quad \theta = \frac{T - T_c}{T_h - T_c}.$$
 (5)

The adjusted set of dimensionless equations is as follows:

$$\frac{\partial U}{\partial x} + \frac{\partial V}{\partial y} = 0,\tag{6}$$

$$U\frac{\partial U}{\partial X} + V\frac{\partial U}{\partial Y} = -\frac{\partial P}{\partial X} + \left(\frac{v_{hnf}}{v_{bf}}\right) \frac{1}{\text{Re}} (\nabla^2 U), \tag{7}$$

$$U\frac{\partial V}{\partial X} + V\frac{\partial V}{\partial Y} = -\frac{\partial P}{\partial Y} + \left(\frac{v_{hnf}}{v_{bf}}\right)\frac{1}{\text{Re}}\left(\nabla^{2}U\right) + \frac{(\rho\beta)_{hnf}}{\rho_{hnf}\beta_{bf}}\text{Ri }\theta - \left(\frac{\rho_{bf}\sigma_{hnf}}{\rho_{hnf}\mu_{bf}}\right)\frac{\text{Ha}^{2}}{\text{Re}}V,$$
(8)

$$U\frac{\partial \theta}{\partial X} + V\frac{\partial \theta}{\partial Y} = \left(\frac{\alpha_{hnf}}{\alpha_{hf}}\right) \frac{1}{\text{Re Pr}} (\nabla^2 \theta), \tag{9}$$

where $\text{Re} = \frac{u_0 L}{\mu_{bf}}$, $\text{Pr} = \frac{v_{bf}}{\alpha_{bf}}$ and $\text{Ha} = \frac{L B_0 \sqrt{\sigma_{bf}}}{\sqrt{\mu_{bf}}}$ represent the Reynolds number, Prandtl number and Hartmann number, respectively. Also, again, $\frac{\text{Gr}}{\text{Re}^2} = \text{Ri}$ is known as the Richardson number, where $\text{Gr} = \frac{g \beta_{bf} (T_h - T_c) L^3}{v_{bf}^2}$ is the Grashoff number. Additionally, the reduced boundary conditions are:

At right circular surface:
$$\theta=1$$
, $U=V=0$ At left circular surface: $\theta=0$, $U=V=0$ Rest of the walls: $\frac{\partial\theta}{\partial N}=0$, $U=V=0$

Furthermore, from the heated left circular surface, the average Nusselt number (Nu_{av}), which is employed to quantify the rate of heat transfer, is obtained by employing:

$$Nu_{av} = -\left(\frac{k_{hnf}}{k_{bf}}\right)_{S} \int \frac{\partial \theta}{\partial N} ds,$$
 (11)

where *S* stands for the surface that is heated, and *N* is the perpendicular unit vector on the *XY*-plane. Moreover, ψ signifies the stream function that is associated by $U = \frac{\partial \psi}{\partial X}$ and $V = \frac{\partial \psi}{\partial Y}$.

Furthermore, $\frac{\partial^2 \psi}{\partial x^2} + \frac{\partial^2 \psi}{\partial y^2} = -\left(\frac{\partial V}{\partial x} - \frac{\partial U}{\partial y}\right) = -\Omega$, where Ω expresses the vorticity vector, and U, V stand for the velocity vector along the X and Y axis, respectively.

3. Numerical methodology

3.1. Solution technique

The dimension-free governing expressions (6) to (9) are mathematically solved utilising the Galerkin weighted residual finite element method (FEM) with boundary settings (10). The entire region is distributed into separate triangular elements, requiring six nodes and accounting for quadratic interpolation functions, in order to monitor the thermal performance and fluid motion. Furthermore, the linear interpolation approach is used to calcu-

late the gradient of pressure. Moreover, the participation of interpolation functions roughly represents the dependent variables of each element as local element coordinates. These equations can be simulated by using the Newton-Raphson iteration method by MATLAB, which generates a set of global nonlinear algebraic equations. In this process, the convergence condition is defined as follows: $\left| \Gamma^{m+1} - \Gamma^m \right| < 10^{-5}$, where m+1 and m stand for two successive repetitions, and $\Gamma(U,V,\theta)$ stands for the iterative value. The complete set of FEM was detailed in [54,55]. The whole flowchart of this computation process is shown in Fig. 2.

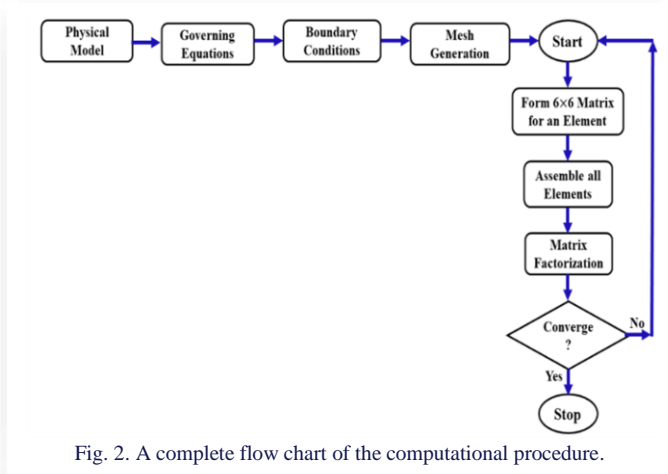


Fig. 2. A complete flow chart of the computational procedure.

This finite element scheme can have the optimal number of elements by taking the following factors into account, which can be determined via a grid sensitivity evaluation. Ri = 1, Ha = 20, Pr = 6.8377, Re = 100, $\phi_{\rm Ag}$ = 0.02 and $\phi_{\rm MgO}$ = 0.02 are the magnitudes. Again, the magnitude of Nu_{av} is designated in order to continue this independence test for meshing. For applying FEM, the entire geometry is subdivided into five distinct triangular elements. These are 2369, 3400, 9570, 27305, and 35665. The computed results of Nu_{av} using FEM for different numbers of triangle members are demonstrated in Table 3 and Fig. 3.

Table 3. Grid independence analysis for the present study.

Elements	2369	3400	9570	27305	35665
Nu _{av}	10.975	11.046	11.207	11.277	11.276

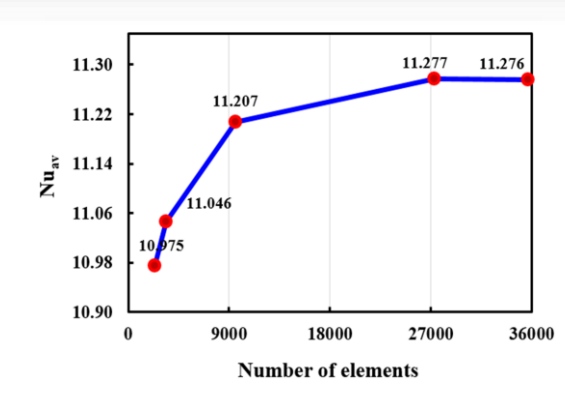


Fig. 3. Grid test by using Nuav and number of elements.

Though for the first three meshing types, the differences are clearly noticeable, it is clear that the magnitude of Nu_{av} for 27305 triangular elements is nearly identical to the cases ensuing a greater number of elements. As a result, 27305 trian-gular elements are selected for discretisation and solving this proposed heat exchanger model.

3.2. Code validation

The purpose of this section is to validate the findings of this study by comparing streamlines and isotherms with those obtained from a lid-driven mixed convective investigation conducted by Sivakumar et al. [56]. To ensure accuracy, the results of Sivakumar's proposed mixed convective heat exchanger model are compared with the present outcomes. The simulation was performed with parameters Re=100, Pr=0.71, and Pr=0.71, within a partially heated square cavity on the left wall, with the right wall maintained at a relatively low temperature and a moving lid on the upper wall. Additionally, we have replicated the work of Sivakumar et al. [56] in this study and compared the streamlines and isotherms (as shown in Fig. 4).

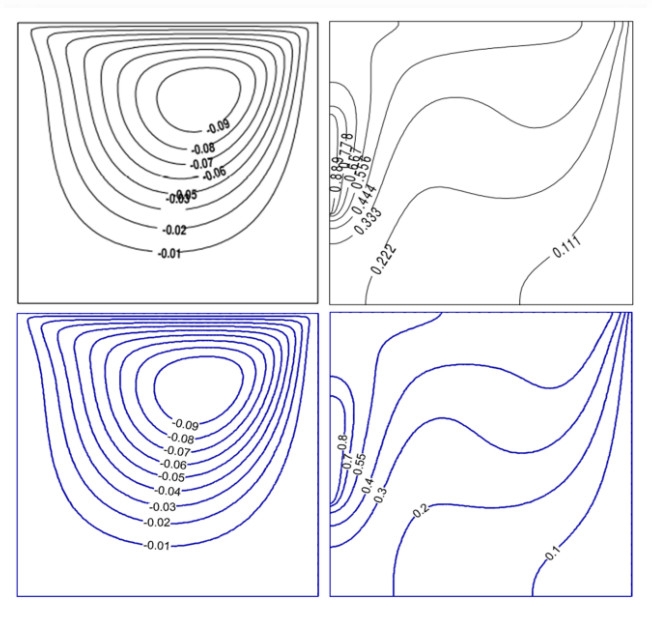


Fig. 4. Comparison of results of Sivakumar et al. [56] (top row) with the current study (bottom row): streamlines (left), isotherms (right).

The top two figures are from Sivakumar's research, while the bottom two are from the current study. The present results closely match the streamline and isotherm patterns, reinforcing our confidence in the accuracy of this mixed convective analysis in near cavities, as it demonstrates strong consistency with the current numerical analysis.

4. Results and discussion

This section explores the effects of physical variables with an engineering focus on trapezoidal mixed convective flow of hybrid nanofluid, including the influence of a magnetic field. The results obtained within this cavity are presented through velocity profiles, streamlines, isotherms, and 2D and 3D response surfaces. The study involves a hybrid nanofluid composed of Ag,

MgO, and H₂O, with spherical solid nanoparticles confined within a trapezoidal chamber. Key parameters such as the Reynolds number (Re), nanoparticle volume fraction (ϕ), Richardson number (Ri), and Hartmann number (Ha) are analysed to show their impact on the heat exchanger model, as in Figs. 5–18. Additionally, the average Nusselt number (Nu_{av}) is used to evaluate the performance of the heat exchanger for water, mono-nano-

fluid, and hybrid nanofluid. For this analysis, standard values for the above-mentioned key parameters are Ri = 1, Ha = 20, Pr = 6.8377, Re = 100, ϕ_{Ag} = 0.02 and ϕ_{MgO} = 0.02.

4.1. Influence of Reynolds number

Figures 5–6 illustrate how the contours of streamlines and isotherms change with varying Reynolds numbers (Re).

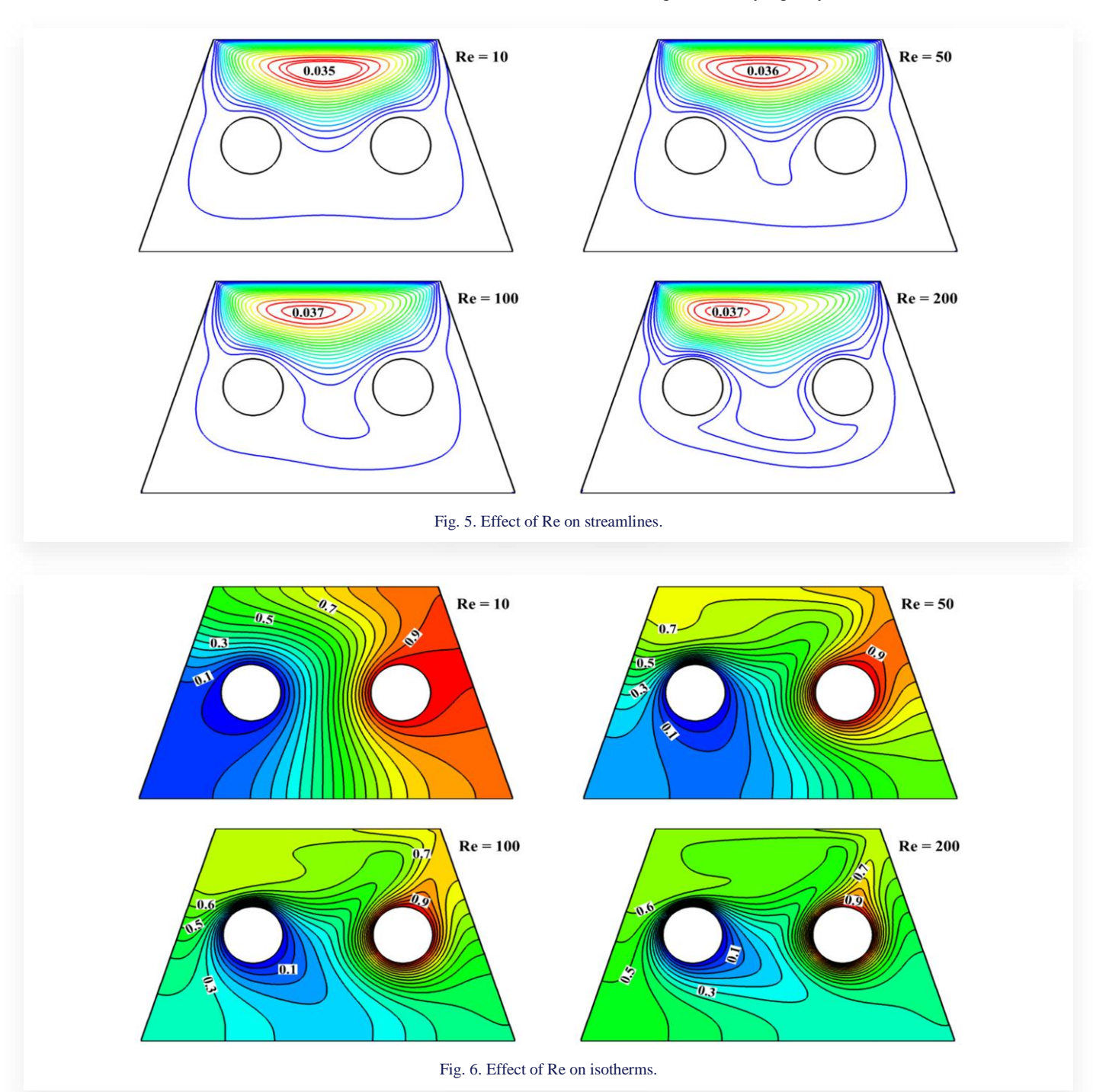
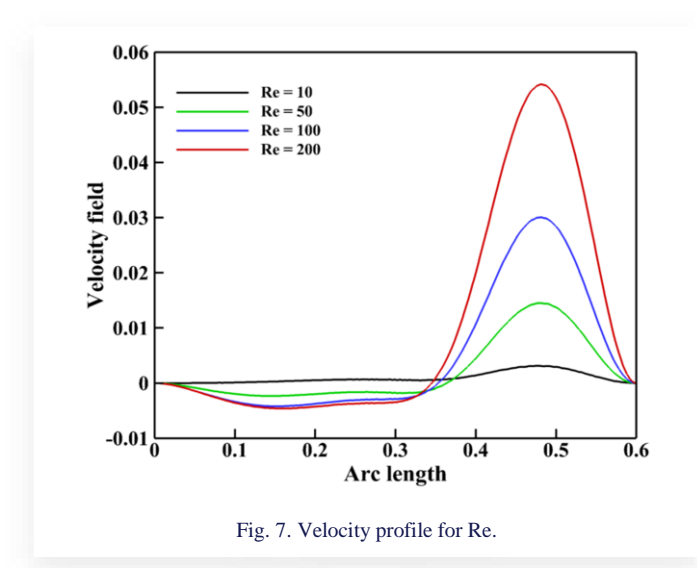


Figure 5 uses streamline contours to demonstrate how Re (10-200) may be controlled for a fluid velocity field when the other parameters are Ri = 1, Ha = 20, Pr = 6.8377 and ϕ_{Ag} = 0.02, ϕ_{MgO} = 0.02. By contrasting the effects of viscous forces and inertia, Re provides insight into the pattern of fluid motion under various circumstances. The streamline concentration and flow

circulation are uniformly circulating throughout the uppermost part of the wall when Re =10. Physically, this is caused by the combined effects of shear force and buoyant force, both of which are controlled at low Re. After that, the streamline vortex and lid velocity both noticeably alter as the Re spikes from 50 to 100. Higher Re values physically result in increased fluid in-

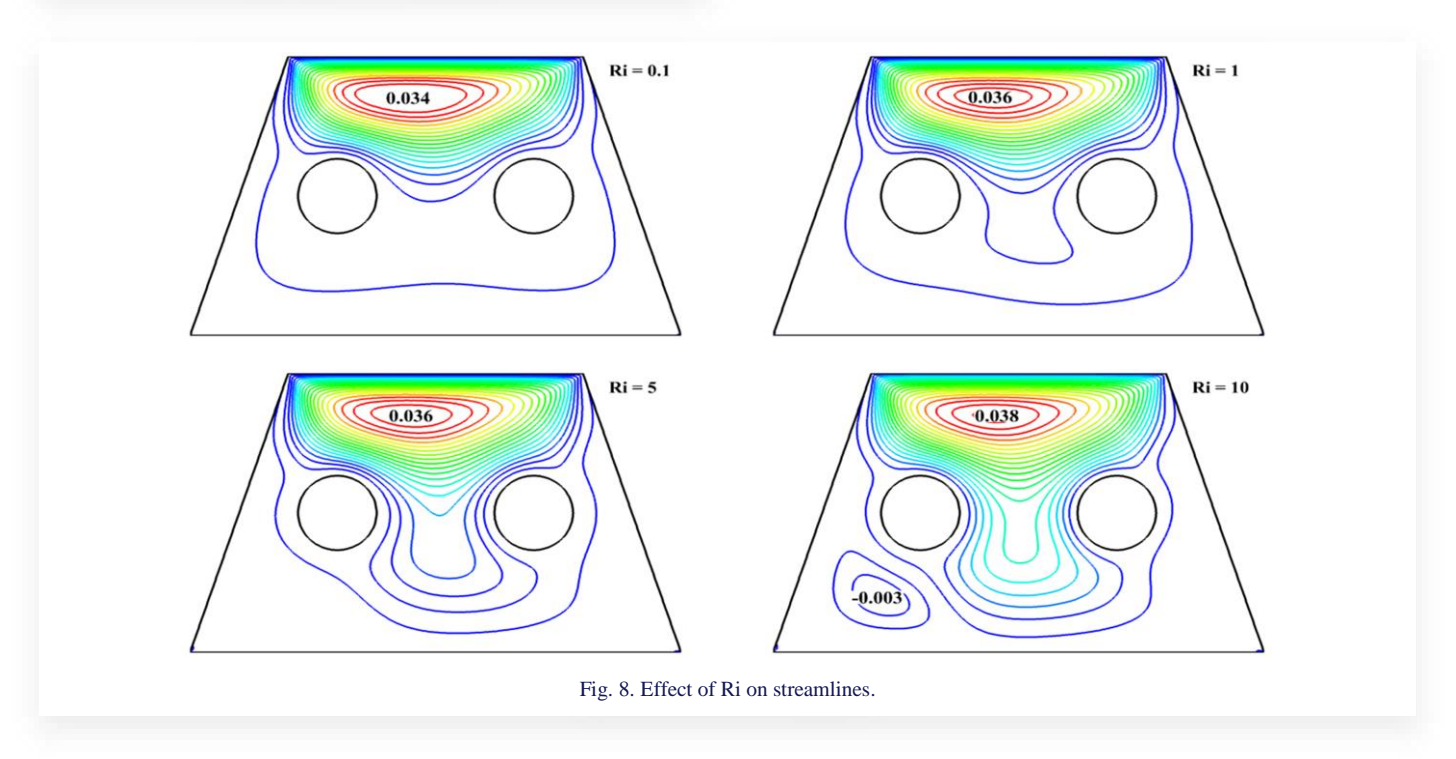
ertia, which raises the flow circulation and magnitude with streamlines concentration. Furthermore, the strengthening of Re signifies the lid velocity of the trapezoidal cavity's top wall; fluid flow follows the lid velocity along the upper wall from the right to the left. The fluid's movement over the upper surface, from right to left, is growing as Re rises. This movement reaches its peak when Re=200. This is because the velocity of the top lid increases with increasing Re, and as a result, forced convection becomes more prominent than sheer force and buoyant force. It is evident that the entire domain experiences an increase in fluid velocity along a line (0.5,0) to (0.5,0.6) as Re develops, which can be seen in Fig. 7.



Moreover, Fig. 6 shows how Re affects the interior isotherms of the cavity. Natural convection is dominant in fluid flow when Re =10. As a result, from the right hot cylinder to the left cooler one, the isotherm lines change uniformly. Force convection occurred, as evidenced by the rising value of Re (50), brought about by the upper wall's rising lid velocity. As can be seen, the red contour lines in the isothermal patterns indicate how fluid movement carries heat from the heated surface to the colder surface. Consequently, there is a 97.07% intensification of heat transmission rate compared to that before. It is apparent, therefore, that when Re rises, the isotherm contour lines distort.

4.2. Influence of Richardson number

The relative significance of forced convection caused by a lid vs. thermal natural convection forces is measured by the Richardson number (Ri) where Ri = Gr/Re². Here, Figs. 8 and 9 are applied to explain the effect of fluid flow and heat transmission using streamlines and isotherms at various Ri values when Re = 100, Ha = 20, Pr = 6.8377, and ϕ_{Ag} = 0.02, ϕ_{MgO} = 0.02. In this investigation, the parameter that has the largest influence on describing the mixed convection is Ri. It is evident from Fig. 8 that the fluid flow pattern is also affected by changes in Ri. Firstly, when Ri = 0.1, a forced convection is evident, with the streamlines moving more along the enclosure's upper wall and to the left. Furthermore, the bulk motion inside the cavity is circulating as a result of the top moving lid's motion, which is caused by the dominance of inertial forces over buoyancy forces. Furthermore, when the forces of buoyancy and inertia are balanced (for Ri = 1), examine the mixed convection mode.



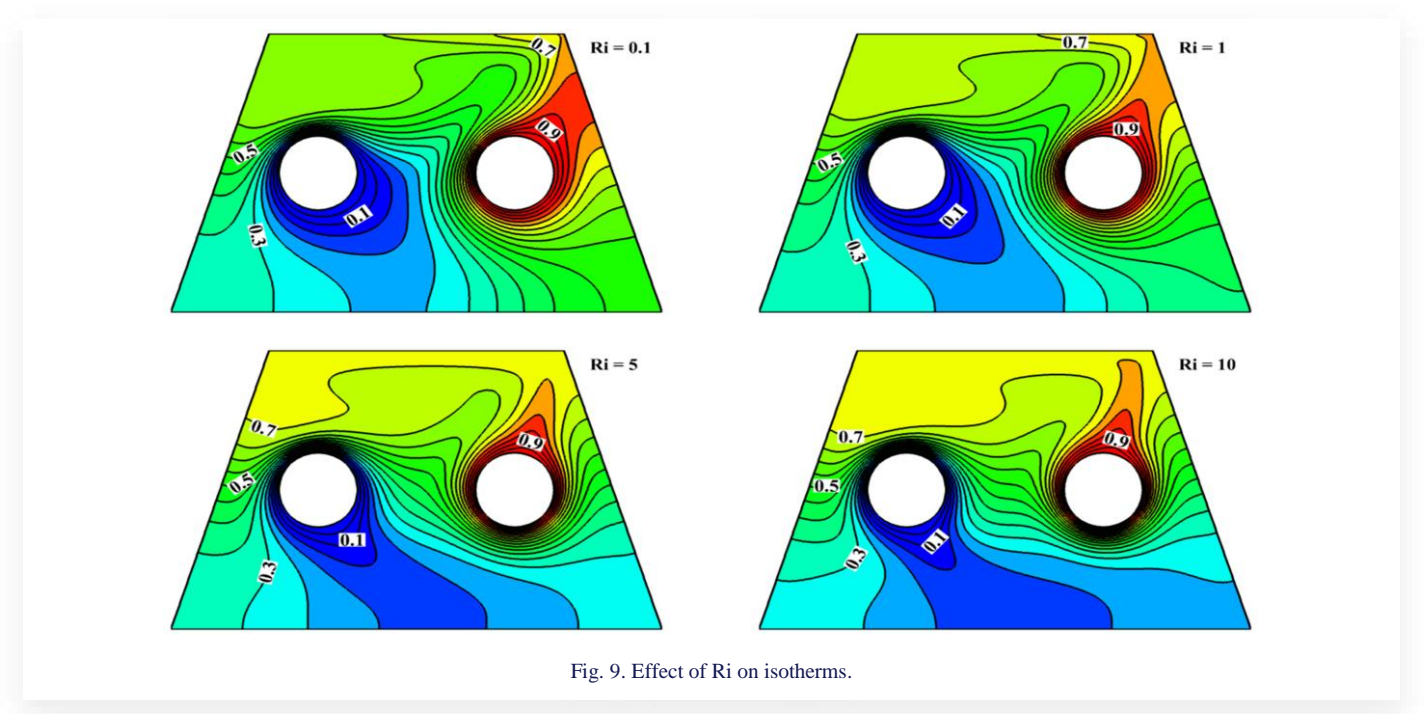
Consequently, the top lid wall experiences a movement effect from the core vortex. Moreover, the streamlines' vortex widens as the value of Ri rises. According to the physical explanation, an escalation of Ri signifies the predominance of natural convection, which reduces shear stress. This created shear stress

provides hurdles for fluid motion. The fluid velocity decreases as the value of Ri rises from 1 to 5, indicating that natural convection is now more significant in this condition.

As a result, the streamlines are shifted somewhat towards the lid wall. A clockwise rotating vortex can be noticed in the cavi-

ty's lower left corner at the highest value of Ri = 10. Also, Fig. 9 illustrates how isotherms are impacted by Ri in the entire trapezoidal cavity. A significant reduction of heat transmission is designated by Nu_{av} of 10.549 at Ri = 0.1. The heat transfer rate rises 6.9% over the lower value prior to the expansion of Ri from 0.1 to 1. Moreover, for Ri = 1, the mixed convection occurs

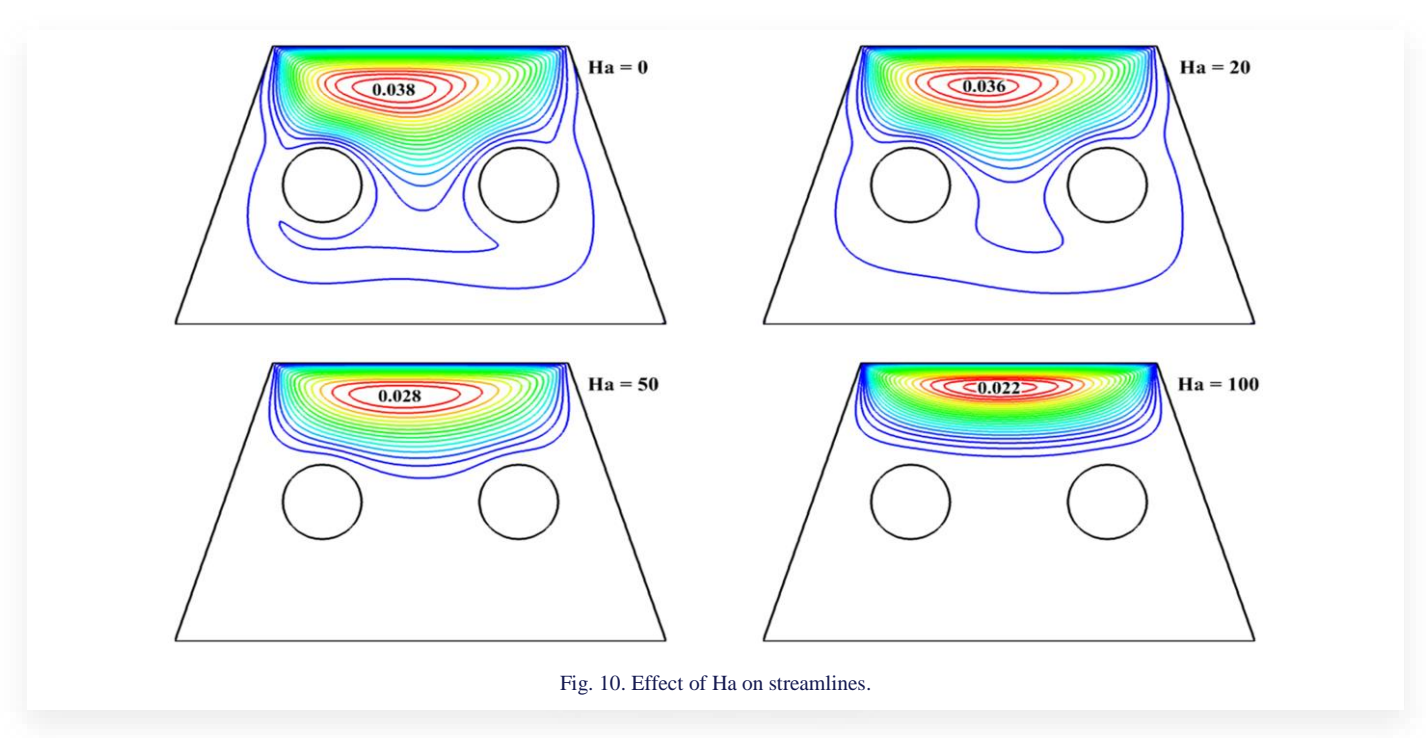
in the entire cavity and at that time Nu_{av} is 11.277. An additional 15.46% enhancement in heat transmission may be seen by increasing Ri from 1 to 5. This analysis shows an increase in Nu_{av} with the enlargement of Ri values. And, there is an 11.16% increase in Nu_{av} as Ri increases from 5 to 10.

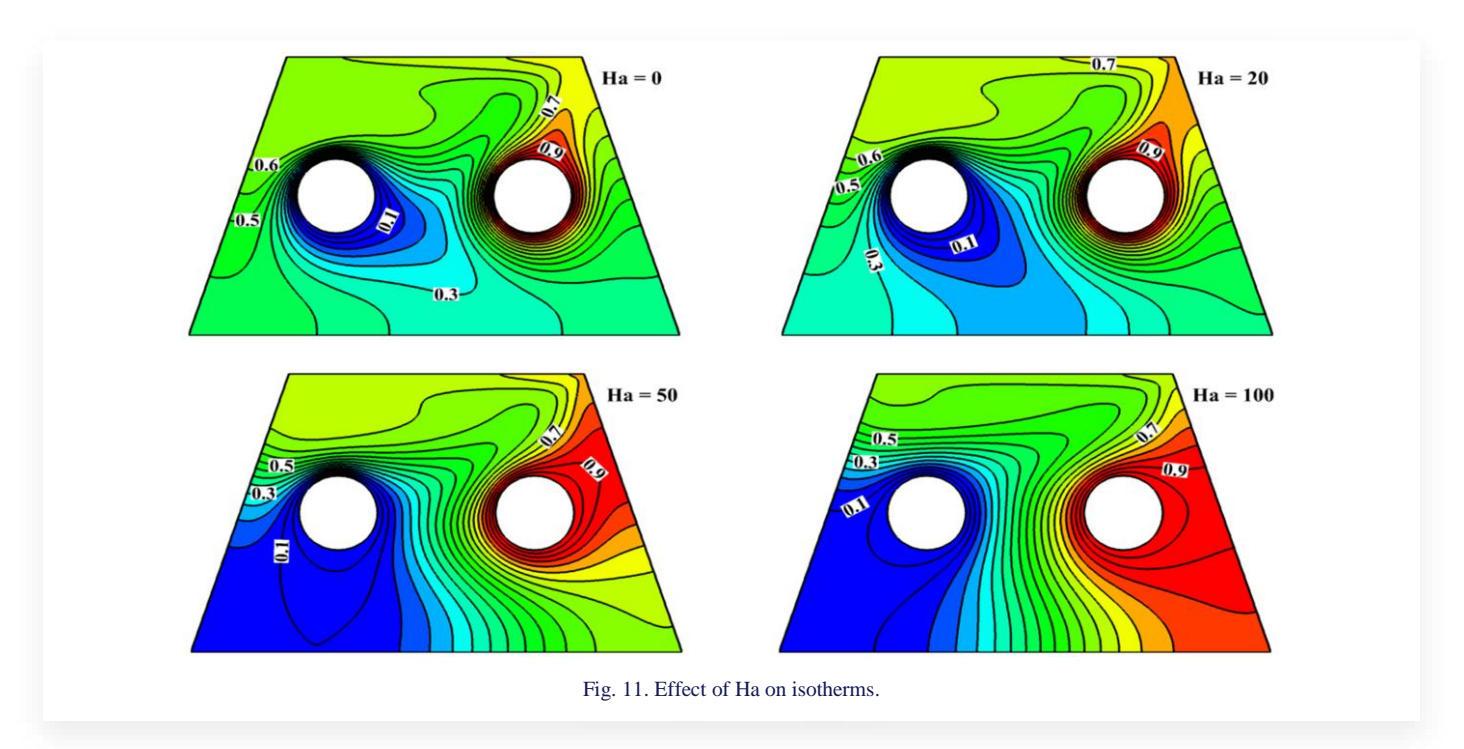


4.3. Influence of Hartmann number

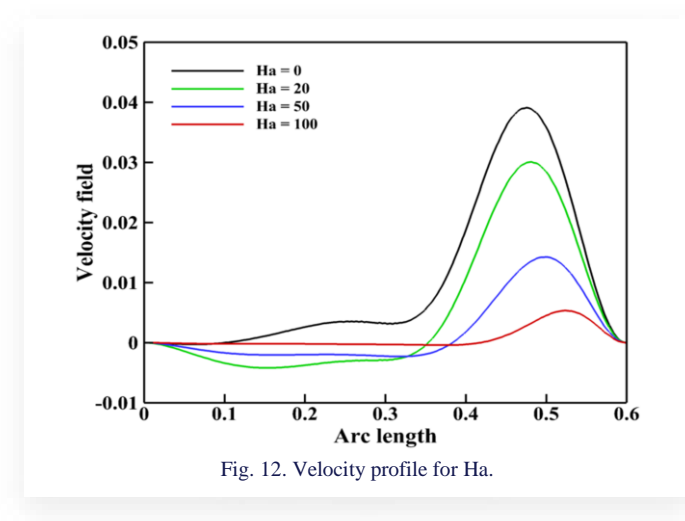
The streamline and isotherm contours in Figs. 10 and 11 demonstrate the consequences of Hartmann number (Ha) on fluid velocity and thermal transportation, keeping Ri = 1, Re = 100, Pr = 6.8377, $\phi_{\rm Ag} = 0.02$ and $\phi_{\rm MgO} = 0.02$. In reality, Ha illustrates how the magnetic force influenced this trapezoidal heat exchanger.

From Fig. 10, the streamline's concentrations are significantly denser without the existence of an external magnetic field (Ha=0). It appears that the flow pattern is consistent across the hollows. However, as the magnitude of fluid vorticity inside the insertion becomes slow, the flow circulation becomes slightly blocked following the intensification of the magnetic field (Ha=20).





It is evident that, in comparison to greater magnetic field effects (Ha = 20, 50, 100), lower magnetic fields (Ha = 0) boost flow behaviour. After increasing the value of Ha from 20 to 50 and from 50 to 100, there is a perceptible effect on the flow circulation. Because of the magnetic force effect, there is an active resistive force inside the enclosure known as the Lorentz force, which has the potential to slow down the mobility of the nanofluid. Precisely, the isotherm lines have a consistent shape in the vertical direction as the convection type of heat transmission progressively gives way to the conduction mode. This physical phenomenon causes the fluid flow to diminish more in the direction of the top lid surface. More importantly, the velocity profile falls with increasing Ha, as Fig. 12 illustrates the velocity profile of Ha. Furthermore, for greater Ha values (Ha = 20, 50, 100), the isothermal lines in Fig. 11 show that the variation of



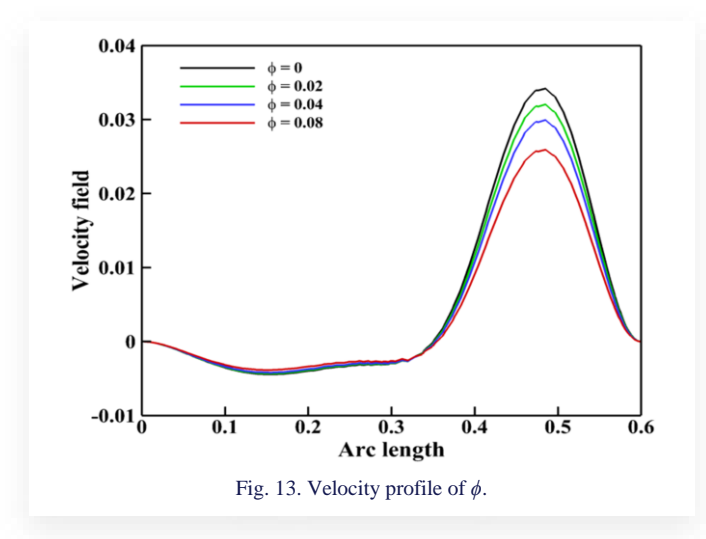
isothermal lines is rather mild (not significant).

When there is no active magnetic field, convectional heat transfer (Nu_{av}) occurs at a high rate. This indicates that due to the addition of magnetic field, the fluid flow meets impedance.

When the value of Ha is enforced from 0 to 20, there is a 7.85% decrease in heat transfer. After the value reached 50, there was a significant decline in heat transfer, around 33.04%. Also, this decreased rate is 31.43% at the maximum magnetic impact value (Ha = 100). The investigation shows that the rate of heat transmission declines at 58.7% from the lowest active magnetic field to the greatest active magnetic field.

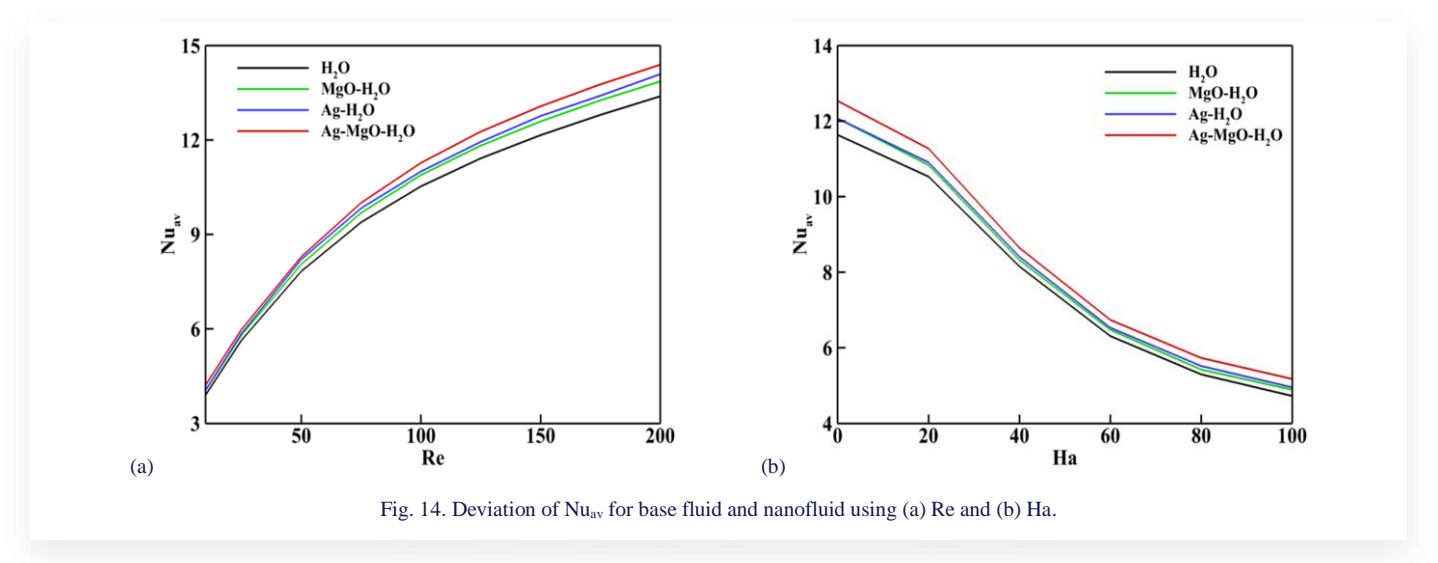
4.4. Importance of nanofluids

This section uses Figs. 13 and 14 to expound the nature of heat transfer and fluid motion on the present model for different magnitudes of the ϕ . Since the velocity profile is therefore controlled by the inherent characteristics of the base fluid, such as density and viscosity, the fluid is a pure base fluid devoid of nanoparticles ($\phi = 0$). The introduction of a modest percentage of nanoparticles ($\phi = 0.02$) really starts to affect the fluid dyna-mics and causes resistance to the particles' mobility in this fluid area. The fluid's inertia force is increased by the cavity's total mass of the fluid. The fluid velocity is significantly reduced as a result of the significant rise in viscosity, which increases flow resistance. An additional factor is that the solution becomes more viscous when more nanoparticles are added. From Fig. 13, it is evident that when ϕ rises, the fluid velocity along the line (0.5, 0) to (0.5, 0.6) decreases significantly. Conversely, the heat transfer rate (Nu_{av}) is rising due to intensification of ϕ , as seen in Fig. 14. The parameters of the base fluid alone dictate Nuav, which is 10.648 in the absence of nanoparticles ($\phi = 0$), as shown by this line graph. Nanoparticle addition begins to marginally increase the heat transfer rate to 3% (10.968) at modest ϕ =0.02. Because of the nanoparticles' increased thermal conductivity, and therefore improved heat transmission within the fluid, there has been an improvement. By increasing the mass of the nanoparticles in the fluid up to 0.04, Nuav is increased by 2.82%. On top of that, compared to $\phi = 0$, Nu_{av} is greatly increased by 11.4% when ϕ is raised by 8% ($\phi = 0.08$).



Superior heat transfer rates arise from the fluid's increased thermal conductivity, which is further enhanced by the high concentration of nanoparticles. Moreover, let's take a look at the significance of accumulation of solid nanoparticles in water more closely (Fig. 14). Here, utilising the properties of Re and Ha, Nu_{av} is used to clarify and illustrate the rate of heat transfer for several fluid types. For pure fluid (H₂O), MgO-H₂O nano-

fluid, Ag-H2O nanofluid and Ag-MgO-H2O hybrid nanofluid, Fig. 14(a) shows that Nu_{av} grows monotonically with the increasing Re. Without the existence of any nanoparticles in water, Nuav is equal to 10.53 by taking all other parameters in a standard form. When $\phi_{\rm MgO} = 0.02$ and $\phi_{\rm Ag} = 0$, adding MgO nanoparticles quickly improves Nu_{av} (10.885) relative to the pure base fluid, which becomes 3.37% greater than that of the base fluid. A similar tendency can be found while adding Ag nanoparticles ($\phi_{MgO} = 0$ and $\phi_{Ag} = 0.02$), which increases the Nu_{av} value relative to the pure base fluid by 3.5% (10.908). But both solid nanoparticles ($\phi_{MgO} = 0.02$ and $\phi_{Ag} = 0.02$) increased Nu_{av} significantly, which is 11.277. This time, the improvement rate is 7.09%. In addition, Fig. 14(b) illustrates how adding mono or hybrid nanoparticles enhances Nu_{av} for distinct values of Ha. The findings indicate that the Ag-MgO-H₂O hybrid nanofluid has a larger Nuav than Ag-H2O nanofluids, yet for all fluid combinations, the rate of Nu_{av} decreases as the Ha factor rises. This indicates that because of the hybrid nanofluid's exceptional thermal properties, the Ag-MgO-H₂O hybrid nanofluid performs better in terms of heat transport than either MgO-H₂O or Ag-H₂O nanofluid. This is the primary reason for utilising hybrid nanofluid as opposed to the base fluid or nanofluid containing a particular nanoparticle.



4.5. Response surface methodology

A well-known statistical analytic technique that explains how the included parameters (Re, ϕ and Ha) impact the response function (Nu_{av}) for this fluid model is called the response surface methodology, or RSM, as described by [57]. This is a useful method for simulating multivariate scenarios in which the input components simultaneously influence the responses that generate interest. Generally, the second-order model produces an acceptable approximation of the response, even in cases where alternative RSM models exist. As per certain accounts, the quadratic RSM model is:

$$y = s_0 + \sum_{i=1}^3 s_i x_i + \sum_{i=1}^3 s_{ii} x_i x_i + \sum_{i=1}^3 s_{ii} x_i^2.$$
 (12)

Here, y is the response function, s_0 , s_i , s_{ij} and s_{ii} are the corresponding terms' coefficients. Here, Nu_{av} is considered the response faction (y), while the significant parameters Re, Ha and

the ϕ function are input parameters. Finding the response function that most closely matches the interaction between independent parts is the primary goal. Here, a second-order RSM model based on central composite design (CCD) is used [58]. This model has 20 runs in total for 3 independent factors: 6 centres, 8 cubes, and 6 axial points per factor. The coded level for CCDbased RSM is shown in Table 4. In addition, Table 5 expresses the real values, response function values, and 20 runs of coded values. The results of this statistical investigation of this model utilising RSM are also displayed in Table 6. The greatest number of autonomous terms is what we refer to as degrees of freedom, or DOF. Moreover, a significant piece of evidence from this analysis is p-value, which reflects the probability that the null hypothesis is accurate for a definite statistical technique. When the p-value is low, it indicates that the null hypothesis is rejected, which indicates that the model is significant. Typically, this is less than 5%.

Table 4. Original and coded levels for CCD-based RSM.

Factors	Coded & original level						
	Lowest value (-1)	Mid value (0)	Lowest value (-1)				
Re	10	105	200				
φ	0	0.04	0.08				
На	0	50	100				

Table 5. Magnitude of the response function for distinct cases.

Run	Co	Coded values			Real values			
Kun	Re	φ	На	Re	φ	На	Nu _{av}	
1	1	0	0	200	0.04	50	10.569	
2	-1	-1	1	10	0	100	3.1986	
3	1	1	-1	200	0.08	0	16.28	
4	0	0	1	105	0.04	100	5.2279	
5	0	1	0	105	0.08	50	8.1926	
6	0	0	0	105	0.04	50	7.7234	
7	1	-1	1	200	0	100	6.0078	
8	-1	1	-1	10	0.08	0	4.8334	
9	0	0	0	105	0.04	50	7.7234	
10	0	0	0	105	0.04	0	12.722	
11	1	1	1	200	0.08	100	6.8295	
12	-1	0	0	10	0.04	50	3.8024	
13	0	0	0	105	0.04	50	7.7234	
14	0	-1	0	105	0	50	7.2798	
15	1	-1	-1	200	0	0	14.227	
16	0	0	0	105	0.04	50	7.7234	
17	-1	1	1	10	0.08	100	3.9276	
18	-1	0	1	10	0.04	100	7.7234	
19	-1	-1	-1	10	0	0	4.2158	
20	0	0	1	105	0.04	100	7.7234	

Table 6. Analysis of variance for Nuav.

Source	DOF	F-value	<i>p</i> -value	Comment
Model	9	38.18	< 0.0001	Significant
Re	1	210.44	< 0.0001	
φ	1	69.67	0.019	
На	1	9.65	< 0.0001	
Re ²	1	7.59	0.0273	
φ ²	1	0.0059	0.3358	
Ha ²	1	0.0317	0.0302	
Re·φ	1	37.64	0.3743	
Re·Ha	1	0.3335	< 0.0001	
<i>φ</i> ·Ha	1	0.5012	0.511	
Lack-of-Fit	5	-	-	Insignificant

Here, $R^2 = 98.53\%$, Adjusted $R^2 = 97.21\%$

The model's statistical analysis and the procedures for testing indicate that the R^2 value (97.85%) for Nu_{av} is superior, indicating that this model is apposite for calculating the response function Nu_{av} , despite having a lower adjusted R^2 value (95.92%). Another crucial statistic that must be exceptionally small for a model to be deemed suitable is lack-of-fit. In order

to investigate the relation between Nu_{av} and the factors Re, Ha and ϕ , a general RSM model is developed as indicated below:

$$y = s_0 + s_1 \text{Re} + s_2 \phi + s_3 \text{Ha} + s_{12} \text{Re} \cdot \phi + s_{13} \text{Re} \cdot \text{Ha} + s_{23} \phi \cdot \text{Ha} + s_{11} \text{Re}^2 + s_{22} \phi^2 + s_{33} \text{Ha}^2,$$
(13)

where s_0 , s_1 , s_2 , s_3 , s_{12} , s_{13} , s_{23} , s_{11} , s_{22} and s_{33} are taken as the coefficients of the regression line concerning Re, Ha and ϕ . Furthermore, Nu_{av}'s anticipated coefficients of Eq. (13) are provided in Table 7 and are calculated as coded units.

Table 7. Coefficients of the regression equation with corresponding *p*-values based on RSM.

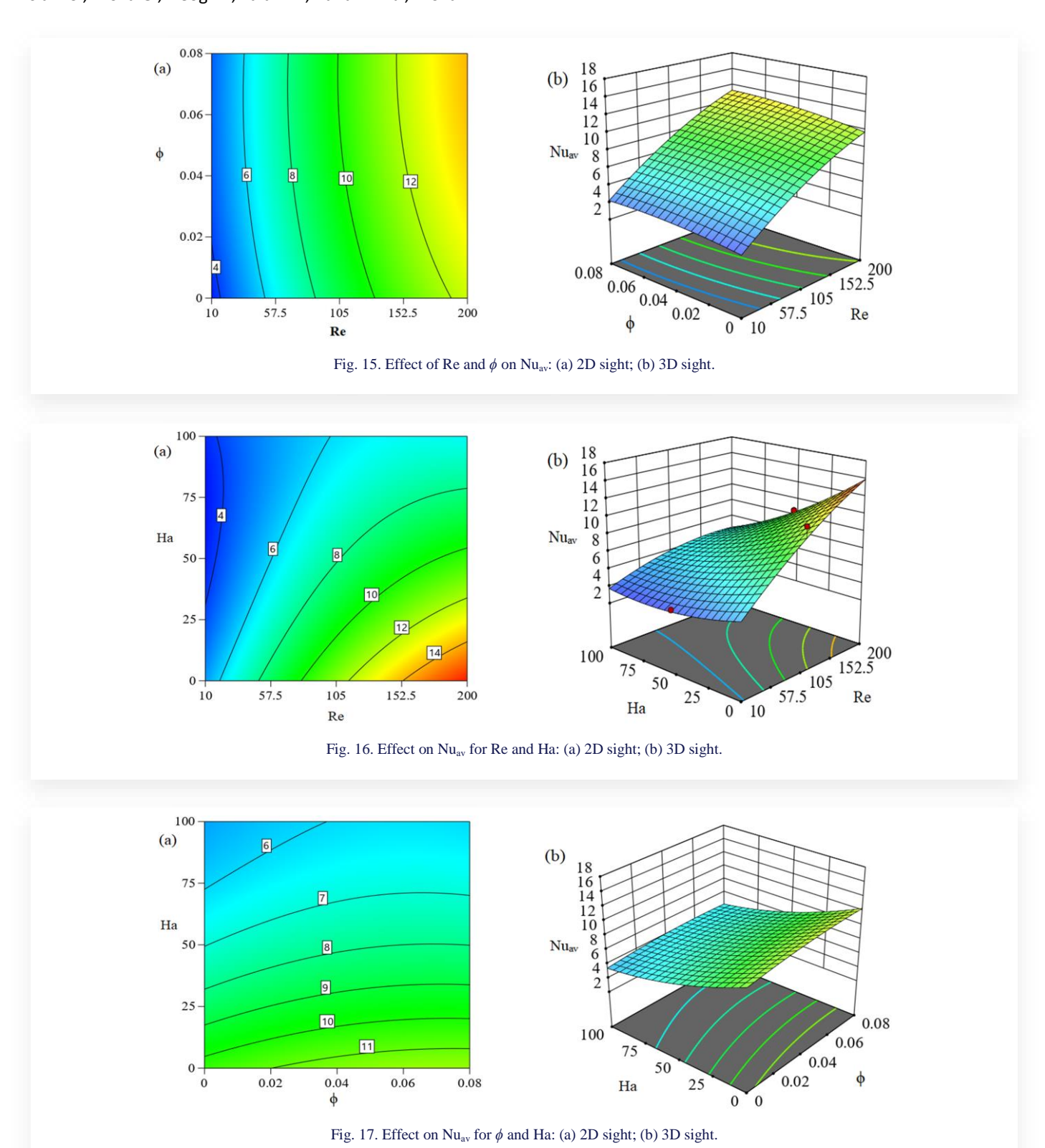
Coefficients	S ₀	S ₁	S ₂	S ₃	S ₁₁
Values	7.87	3.39	0.5134	-2.71	-0.905
p-values	-	<0.0001	0.019	<0.0001	0.0273
Coefficients	S ₂₂	S ₃₃	S ₁₂	S ₁₃	S ₂₃
Values	-0.3545	0.8842	0.1910	-1.97	-0.14
<i>p</i> -values	0.3358	0.0302	0.3743	< 0.0001	0.511

A suitable regression equation has only been developed utilising the significant model terms with lower p-values, owing to their importance. On the contrary, the terms that are not essential have been neglected (bold emphasised). Therefore, the terms ϕ^2 , Re· ϕ and ϕ ·Ha have no influence whatsoever on Nu_{av}'s regression equation (13). Consequently, the subsequent mathematical correlation can be applied to relate Nu_{av} with the parameters Re, ϕ and Ha:

$$Nu_{av} = 7.87 + 3.39Re + 0.5134\phi - 2.71Ha - 0.905Re^2 + 0.8842Ha^2 - 1.97Re \cdot Ha.$$
 (14)

4.6. Response surface analysis

With a view to analysing the influence of independent components on the response function, in this segment, Figs. 15–17 provide 2D and 3D contour plots regarding the response surface developed using RSM (Nu_{av}). Figure 15(a) demonstrates Nu_{av}'s reaction to Re and ϕ . This 2D contour map clearly illustrates that the response function rises with both Re and ϕ . For example, the rate of heat transmission proliferations increases by about 103.1% when the value of Re goes up from 10 (coded value 1) to 105 (coded value 0). At this point, Nuav grows by around 36.84% when the magnitude of Re is raised from 105 (coded value 0) to 200 (coded value 1). At the greatest magnitude of Re and ϕ (coded value 1), the fluctuating rate of Nu_{av} is maximal, as seen in the 2D contours in Fig. 15(a). Moreover, Fig. 15(b) displays a 3D surface plot of the effects of Re and ϕ on Nu_{av}. Moreover, several 2D and 3D graphical representations are also shown in Fig. 16(a) to show how Re and Ha influence Nu_{av} in this hybrid nanofluid model. Furthermore, although ϕ remains constant, a rise in Ha diminishes the rate of Nu_{av}. Additionally, Fig. 16(b) displays a 3D surface depiction of Re and Ha's effects on Nu_{av}. Likewise, Fig. 17 illustrates Nu_{av}'s impact from Ha and ϕ . Here, the altering rate of Nu_{av} is advanced by increasing the size of ϕ while decreasing the magnetic field. Nu_{av}'s fluctuating rate is lower than it was in the prior two cases, though.



4.7. Sensitivity analysis of parameters

Sensitivity analysis, a process for the determination of how input uncertainty affects the model's response, is crucial to numerical simulation. By doing a "sensitivity analysis", it is possible to determine the extent to which the model's parameter distresses the generated variables [59]. Using the results of the sensitivity analysis, the important variables can be ranked in order of influence to determine which parameter is the most beneficial. By

differentiating (partially) the response function with respect to autonomous factors (Re, ϕ and Ha), one can analytically evaluate the sensitivity of the output. Consequently, the following computation is made for Nu_{av} with respect to the input parameters as in Eq. (14):

$$\frac{\partial \text{Nu}_{av}}{\partial \text{Re}} = 3.39 - 1.81\text{Re} - 1.97\text{Ha},$$
 (15)

$$\frac{\partial Nu_{av}}{\partial \phi} = 0.5134,\tag{16}$$

$$\frac{\partial \text{Nu}_{av}}{\partial \text{Ha}} = -2.71 + 1.7684 \text{Ha} - 1.97 \text{Re}. \tag{17}$$

Eqs. (15) to (17) can now be used to calculate the rate of sensitivity of Nu_{av} to Re, ϕ and Ha. Table 8 presents the findings.

Table 8. Sensitivity analysis for Nu_{av}.

Re	φ	На	$\frac{\partial Nu_{av}}{\partial Re}$	$\frac{\partial \mathrm{Nu}_{av}}{\partial \phi}$	$\frac{\partial \mathrm{Nu}_{av}}{\partial \mathrm{Ha}}$
-1		-1	7.17	0.5134	-0.226
-1		0	5.2	0.5134	-0.74
0	0	-1	5.36	0.5134	-4.478
		0	3.39	0.5134	-2.71
1		-1	3.55	0.5134	-6.448
1		0	1.58	0.5134	-4.68
-1		-1	7.17	0.5134	-0.226
-1		0	5.2	0.5134	74
0	1	-1	5.36	0.5134	-4.478
U	1	0	3.39	0.5134	-2.71
1		-1	3.55	0.5134	-6.448
1		0	1.58	0.5134	-4.68

The values obtained by applying this model are as follows: Ha at -1 and 0 (0 and 50), ϕ at 0 and 1 (0.04 and 0.08), and Re at -1, 0 and 1 (10, 105 and 200). Furthermore, it's critical to remember that a positive sensitivity indicates that the input factors are intensifying this response. This demonstrates how the Re and ϕ stimulate Nu_{av} in a positive way. Conversely, a negative sensitivity signifies the exact opposite trend, where raising input factors causes the response to drop. This signal suggests that the input factor Ha has a negative effect on Nu_{av}. Moreover, Fig. 18 illustrates negative sensitivity with respect to Nu_{av} by the flipped bar and positive sensitivity with respect to Nu_{av} by the upright bar. The sensitivity level is also displayed along the entire length of the bar.

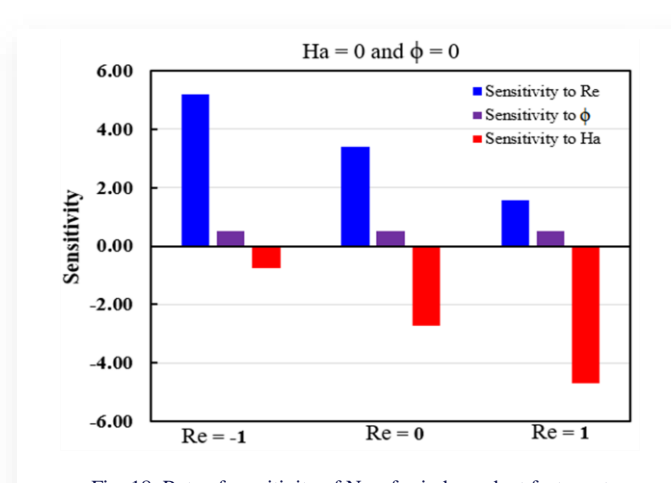


Fig. 18. Rate of sensitivity of Nu_{av} for independent factors at Ha = 0 and ϕ = 0.

6. Conclusions

This study focuses on the interaction between heat transport processes and the effects of magnetic fields, examining the behaviour of mixed convective heat fluxes in a confined cavity using a hybrid (Ag-MgO-H₂O) nanofluid. A numerical solution is developed using the Galerkin finite element method to capture the complex behaviour. The key findings are outlined below:

- Sensitivity analysis of the response function is performed using RSM to gain a comprehensive understanding of the heat transportation mechanism.
- The impact of the hybrid nanofluid on streamlines, isotherms, and Nu_{av} is investigated.
- Surface plots in two and three dimensions provide a clear visual representation of the heat transmission process for significant components involved.
- The hybrid nanofluid (Ag-MgO-H2O) shows superior thermal properties, resulting in better heat transfer performance than the base fluid or mono nanofluid, with heat transfer improvements of 3.37% and 7.09%, respectively.
- The Hartmann number (Ha) has a negative impact on the velocity profile.
- Sensitivity analysis results show that Reynolds number (Re) and nanoparticle volume fraction (φ) positively influence heat transfer from hot surfaces, while Ha has a negative impact on it.

This study can be extended in the future for non-Newtonian fluids and temperature-dependent thermophysical properties with a three-dimensional approach.

Acknowledgements

This research received funding BSMRSTU-RC-24-024, 2023–2024, from Bangabandhu Sheikh Mujibur Rahman Science and Technology University, Gopalganj 8100, Bangladesh.

References

- [1] Cha, C.K., & Jaluria, Y. (1984). Recirculating mixed convection flow for energy extraction. *International Journal of Heat and Mass Transfer*, 27(10), 1801–1812. doi: 10.1016/0017-9310(84) 90162-5
- [2] Sadeghi, H.M., Babayan, M., & Chamkha, A. (2020). Investigation of using multi-layer PCMs in the tubular heat exchanger with periodic heat transfer boundary condition. *International Journal of Heat and Mass Transfer*, 147, 118970. doi: 10.1016/j. ijheatmasstransfer.2019.118970
- [3] Qureshi, M.A., Hussain, S., & Sadiq, M.A. (2021). Numerical simulations of MHD mixed convection of hybrid nanofluid flow in a horizontal channel with cavity: Impact on heat transfer and hydrodynamic forces. *Case Studies in Thermal Engineering*, 27, 101321. doi: 10.1016/j.csite.2021.101321
- [4] Islam, S., Islam, M.M., Rana, B.M.J., Islam, M.S., Reza-E-Rabbi, S., Hossain, M.S., & Rahman, M.M. (2023). Numerical investigation with sensitivity study of MHD mixed convective hexagonal heat exchanger using TiO₂–H₂O nanofluid. *Results in Engineering*, 18, 101136. doi: 10.1016/j.rineng.2023.101136
- [5] Mahalakshmi, T. (2023). A numerical analysis on MHD mixed convective hybrid nanofluid flow inside enclosure with heat

- sources. *Journal of Nanofluids*, 12(4), 942–954. doi: 10.1166/jon.2023.1975
- [6] Choi, S.U., & Eastman, J.A. (1995). Enhancing thermal conductivity of fluids with nanoparticles (No. ANL/MSD/CP-84938; CONF-951135-29). Argonne National Lab. (ANL), Argonne, IL (United States).
- [7] Nadeem, S., Abbas, N., & Malik, M.Y. (2020). Inspection of hybrid based nanofluid flow over a curved surface. *Computer methods and programs in biomedicine*, 189, 105193. doi: 10.1016/j.cmpb.2019.105193
- [8] Habiba, U., Hudha, M.N., Neogi, B., Islam, S., & Rahman, M.M. (2025). Numerical exploration on n-decane nanofluid based MHD mixed convection in a lid driven cavity: impact of magnetic field and thermal radiation. *International Journal of Thermofluids*, 27, 101209. doi.org/10.1016/j.ijft.2025.101209
- [9] Kaushik, S., Singh Mahar, V., Singh, S., Kshetri, R., Kumar, B., Singh Mehta, J., & Kumar, A. (2024). Comparative experimental analysis of fluid flow in a concentric tube exchanger having semi hollow cylindrical macro inserts with nanofluid and base fluid. *Archives of Thermodynamics*, 45(2). doi: 10.24425/ather.2024. 150866
- [10] Islam, S., Siddiki, M.N.A.A., & Islam, M.S. (2024). Numerical simulation and sensitivity analysis using RSM on natural convective heat exchanger containing hybrid nanofluids. *Mathematical Problems in Engineering*, 2024(1), 2834556. doi: 10.1155/2024/ 2834556
- [11] Dogonchi, A.S., Chamkha, A.J., & Ganji, D.D. (2019). A numerical investigation of magneto-hydrodynamic natural convection of Cu–water nanofluid in a wavy cavity using CVFEM. *Journal of Thermal Analysis and Calorimetry*, 135(4), 2599–2611. doi: 10.1007/s10973-018-7339-z
- [12] Siddiki, M.N.A.A., Islam, S., Ahmmed, M.U., & Molla, M.M. (2024). Numerical simulation of a non-Newtonian nanofluid on mixed convection in a rectangular enclosure with two rotating cylinders. *International Journal of Ambient Energy*, 45(1), 2332525. doi: 10.1080/01430750.2024.2332525
- [13] Hashemi-Tilehnoee, M., Dogonchi, A.S., Seyyedi, S.M., Chamkha, A.J., & Ganji, D.D. (2020). Magnetohydrodynamic natural convection and entropy generation analyses inside a nanofluid-filled incinerator-shaped porous cavity with wavy heater block. *Journal of Thermal Analysis and Calorimetry*, 141(5), 2033–2045. doi: 10.1007/s10973-019-09220-6
- [14] Acharya, N., & Chamkha, A.J. (2022). On the magnetohydrodynamic Al2O3-water nanofluid flow through parallel fins enclosed inside a partially heated hexagonal cavity. *International Communications in Heat and Mass Transfer*, 132, 105885. doi: 10.1016/j.icheatmasstransfer.2022.105885
- [15] Wang, D., & Hai, T. (2023). Effect of the length and thickness of three constant temperature baffles on the natural convection heat transfer of nanofluid flow inside an enclosure affected by a magnetic field. *Engineering Analysis with Boundary Elements*, 150, 70–83. doi: 10.1016/j.enganabound.2023.01.038
- [16] Kaushik, S., Uniyal, V., Verma, A.K., Jha, A.K., Joshi, S., Makhloga, M., Pargai, P.S., Sharma, S.K., Kumar, R., & Pal, S. (2023). Comparative experimental and cfd analysis of fluid flow attributes in mini channel with hybrid CuO+ Zno+ H₂O nano fluid and (H2O) base fluid. EVERGREEN Joint Journal of Novel Carbon Resource Sciences and Green Asia Strategy, 10(1), 182–195. doi: 10.5109/6781069
- [17] Hussain, S., Ahmed, S.E., & Akbar, T. (2017). Entropy generation analysis in MHD mixed convection of hybrid nanofluid in an open cavity with a horizontal channel containing an adiabatic obstacle. *International Journal of Heat and Mass Transfer*, 114, 1054–1066. doi: 10.1016/j.ijheatmasstransfer.2017.06.135

- [18] Zaboli, M., Ajarostaghi, S.S.M., Saedodin, S., & Kiani, B. (2021). Hybrid nanofluid flow and heat transfer in a parabolic trough solar collector with inner helical axial fins as turbulator. *The European Physical Journal Plus*, 136(8), 841. doi: 10.1140/epip/s13360-021-01807-z
- [19] Mahalakshmi, T. (2023). A numerical analysis on MHD mixed convective hybrid nanofluid flow inside enclosure with heat sources. *Journal of Nanofluids*, 12(4), 942–954. doi: 10.1166/jon.2023.1975
- [20] Mandal, D.K., Biswas, N., Manna, N.K., Gorla, R.S.R., & Chamkha, A.J. (2023). Hybrid nanofluid magnetohydrodynamic mixed convection in a novel W-shaped porous system. *International Journal of Numerical Methods for Heat and Fluid Flow*, 33(2), 510–544. doi: 10.1108/HFF-03-2022-0163
- [21] Anee, M.J., Hasan, M.F., Siddiqa, S., & Molla, M.M. (2024). MHD Natural Convection and Sensitivity Analysis of Ethylene Glycol Cu-Al₂O₃ Hybrid Nanofluids in a Chamber with Multiple Heaters: A Numerical Study of Lattice Boltzmann Method. *International Journal of Energy Research*, 2024(1), 5521610. doi: 10.1155/2024/5521610
- [22] Thumma, T., Pyari, D.R., Ontela, S., Al-Mdallal, Q.M., & Jarad, F. (2023). Heat transfer analysis of magnetized Cu-Ag-H₂O hybrid nanofluid radiative flow over a spinning disk when the exponential heat source and Hall current are substantial: optimization and sensitivity analysis. *Case Studies in Thermal Engineering*, 50, 103448. doi: 10.1016/j.csite.2023.103448
- [23] Sheikholeslami, M. (2019). New computational approach for exergy and entropy analysis of nanofluid under the impact of Lorentz force through a porous media. *Computer Methods in Applied Mechanics and Engineering*, 344, 319–333. doi: 10.1016/j.cma.2018.09.044
- [24] Khatun, S., Kundu, R., Islam, S., Aktary, R., & Kumar, D. (2025). Sensitivity analysis on natural convective trapezoidal cavity containing hybrid nanofluid with magnetic effect: Numerical and statistical approach. *Heliyon*, 11(1). doi: 10.1016/j.heliyon.2024. e41508
- [25] Ali, M.Y., Islam, S., Alim, M.A., Biplob, R.A., & Islam, M.Z. (2024). Numerical investigation of MHD mixed convection in an octagonal heat exchanger containing hybrid nanofluid. *Heliyon*, 10(17).doi: 10.1016/j.heliyon.2024.e37162
- [26] Alahmadi, R.A., Raza, J., Mushtaq, T., Abdelmohsen, S.A., Gorji, M.R., & Hassan, A. M. (2023). Optimization of MHD flow of radiative micropolar nanofluid in a channel by RSM: sensitivity analysis. *Mathematics*, 11(4), 939. doi: 10.3390/ math11040939
- [27] Neogi, B., Islam, S., Faiaz, M., Rana, B.J., & Rahman, M.M. (2025). Numerical exploration and sensitivity analysis on MHD natural convective hexagonal enclosure using Ag-MgO-H₂O hybrid nanofluids. *International Journal of Ambient Energy*, 46(1), 2444369. doi: 10.1080/01430750.2024.2444369
- [28] Tayebi, T., & Chamkha, A.J. (2020). Magnetohydrodynamic natural convection heat transfer of hybrid nanofluid in a square enclosure in the presence of a wavy circular conductive cylinder. *Journal of Thermal Science and Engineering Applications*, 12(3), 031009. doi: 10.1115/1.4044857
- [29] Gibanov, N.S., Sheremet, M.A., Oztop, H.F., & Abu-Hamdeh, N. (2017). Effect of uniform inclined magnetic field on mixed convection in a lid-driven cavity having a horizontal porous layer saturated with a ferrofluid. *International Journal of Heat and Mass Transfer*, 114, 1086–1097. doi: 10.1016/j.ijheatmasstrans-fer. 2017.07.001
- [30] Mebarek-Oudina, F., Redouane, F., & Rajashekhar, C. (2020). Convection heat transfer of MgO-Ag/water magneto-hybrid nanoliquid flow into a special porous enclosure. Algerian Journal

- of Renewable Energy and Sustainable Development, 2(2), 84–95. doi: 10.46657/ajresd.2020.2.2.1
- [31] Selimefendigil, F., & Chamkha, A.J. (2021). MHD mixed convection of Ag–MgO/water nanofluid in a triangular shape partitioned lid-driven square cavity involving a porous compound. *Journal of Thermal Analysis and Calorimetry*, 143(2), 1467–1484. doi: 10.1007/s10973-020-09472-7
- [32] Ma, Y., Rashidi, M.M., Mohebbi, R., & Yang, Z. (2021). Investigation of magnetohydrodynamics in Ag-TiO₂/water hybrid nanofluid in a Shamse knot shaped cavity. *International Journal of Numerical Methods for Heat and Fluid Flow*, 31(1), 251–272. doi: 10.1108/HFF-12-2019-0909
- [33] Munawar, S., Saleem, N., Ahmad Khan, W., & Nasir, S. (2021). Mixed convection of hybrid nanofluid in an inclined enclosure with a circular center heater under inclined magnetic field. *Coatings*, 11(5), 506. doi: 10.3390/coatings11050506
- [34] Mourad, A., Aissa, A., Mebarek-Oudina, F., Jamshed, W., Ahmed, W., Ali, H.M., & Rashad, A.M. (2021). Galerkin finite element analysis of thermal aspects of Fe₃O₄-MWCNT/water hybrid nanofluid filled in wavy enclosure with uniform magnetic field effect. *International Communications in Heat and Mass Transfer*, 126, 105461. doi: 10.1016/j.icheatmasstransfer.2021. 105461
- [35] Kaushik, S., Singh, S., & Panwar, K. (2021). Comparative analysis of thermal and fluid flow behaviour of diverse nano fluid using Al₂O₃, ZnO, CuO nano materials in concentric spiral tube heat exchanger. *Materials Today: Proceedings*, 46, 6625–6630. doi: 10.1016/j.matpr.2022.10.117
- [36] Zhang, Y., Hangi, M., Wang, X., & Rahbari, A. (2023). A comparative evaluation of double-pipe heat exchangers with enhanced mixing. *Applied Thermal Engineering*, 230, 120793. doi: 10.1016/j.applthermaleng.2023.120793
- [37] Kaushik, S., Singh, S., & Panwar, K. (2023). Experimental study of fluid flow properties in spiral tube heat exchanger with varying insert shape over spiral tube profile. *Materials Today: Proceedings*, 80, 78–84. doi: 10.1016/j.matpr.2022.10.117
- [38] Tian, G., Tian, C., Alizadeh, A.A., Shirani, N., Nasajpour-Esfahani, N., Shamsborhan, M., & Baghaei, S. (2023). Entropy analysis and mixed convection of nanofluid flow in a pillow plate heat exchanger in the presence of porous medium. *Alexandria Engineering Journal*, 82, 541–556. doi: 10.1016/j.aej.2023. 10.019
- [39] Kaushik, S., Singh, S., Kanojia, N., Rawat, K., & Panwar, K. (2020, March). Comparative study for thermal and fluid flow peculiarities in cascading spiral inner tube heat exchanger with or without diverse inserts over spiral tube. In *IOP Conference Series: Materials Science and Engineering*, 802(1), 012009. doi: 10.1088/1757-899X/802/1/012009
- [40] Chen, H.T., Lin, Y.S., Chen, P.C., & Chang, J.R. (2016). Numerical and experimental study of natural convection heat transfer characteristics for vertical plate fin and tube heat exchangers with various tube diameters. *International Journal of Heat and Mass Transfer*, 100, 320–331. doi: 10.1016/j. ijheatmasstransfer.2016. 04.039
- [41] Lee, J.H., Shin, J.H., Chang, S.M., & Min, T. (2020). Numerical analysis on natural convection heat transfer in a single circular fin-tube heat exchanger (Part 1): numerical method. *Entropy*, 22(3), 363. doi: 10.3390/e22030363
- [42] Pakalka, S., Valančius, K., & Streckienė, G. (2021). Experimental and theoretical investigation of the natural convection heat transfer coefficient in phase change material (PCM) based fin-and-tube heat exchanger. *Energies*, 14(3), 716. doi: 10.3390/en14030716
- [43] Haq, R.U., Soomro, F.A., Wang, X., & Tlili, I. (2020). Partially heated lid-driven flow in a hexagonal cavity with inner circular obstacle via FEM. *International Communications in Heat and*

- *Mass Transfer*, 117, 104732. doi: 10.1016/j.icheatmasstransfer. 2020.104732
- [44] Toudja, N., Labsi, N., Benkahla, Y.K., Ouyahia, S.E., & Benzema, M. (2022). Thermosolutal mixed convection in a lid-driven irregular hexagon cavity filled with MWCNT-MgO (15–85%)/CMC non-Newtonian hybrid nanofluid. *Journal of Thermal Analysis and Calorimetry*, 147, 855–878. doi: 10.1007/s10973-020-10288-8
- [45] Rehman, K.U., Malik, M.Y., Al-Mdallal, Q.M., & Al-Kouz, W. (2020). Heat transfer analysis on buoyantly convective non-Newtonian stream in a hexagonal enclosure rooted with T-Shaped flipper: hybrid meshed analysis. *Case Studies in Thermal Engineering*, 21, 100725. doi: 10.1016/j.csite.2020.100725
- [46] Majeed, A.H., Mahmood, R., Shahzad, H., Pasha, A.A., Islam, N., & Rahman, M.M. (2022). Numerical simulation of thermal flows and entropy generation of magnetized hybrid nanomaterials filled in a hexagonal cavity. *Case Studies in Thermal Engineering*, 39, 102293. doi: 10.1016/j.csite.2022.102293
- [47] Garoosi, F., Hoseininejad, F., & Rashidi, M.M. (2016). Numerical study of heat transfer performance of nanofluids in a heat exchanger. *Applied Thermal Engineering*, 105, 436–455. doi: 10.1016/j.applthermaleng.2016.03.015
- [48] Goodarzi, M., D'Orazio, A., Keshavarzi, A., Mousavi, S., & Karimipour, A. (2018). Develop the nano scale method of lattice Boltzmann to predict the fluid flow and heat transfer of air in the inclined lid driven cavity with a large heat source inside, Two case studies: Pure natural convection & mixed convection. *Physica A: Statistical Mechanics and Its Applications*, 509, 210–233. doi: 10.1016/j.physa.2018.06.013
- [49] Plant, R.D., & Saghir, M.Z. (2021). Numerical and experimental investigation of high concentration aqueous alumina nanofluids in a two and three channel heat exchanger. *International Journal of Thermofluids*, 9, 100055. doi: 10.1016/j.ijft.2020.100055
- [50] Hirpho, M., & Ibrahim, W. (2022). Mixed convection heat transfer of a hybrid nanofluid in a trapezoidal prism with an adiabatic circular cylinder. *Mathematical Problems in Engineering*, 2022(1), 8170224. doi: 10.1155/2022/8170224
- [51] Aktary, R., Islam, S., Ray, S.C., Khatun, S., Kundu, R., & Biswas, A. (2025). Thermal performance analysis of Cu-MgO-H2O hybrid nanofluid in a partially heated trapezoidal cavity: FEM, RSM and ANN approaches. *Thermal Advances*, 4, 100062. doi.org/10.1016/j.thradv.2025.100062
- [52] Chabani, I., Mebarek-Oudina, F., Vaidya, H., & Ismail, A.I. (2022). Numerical analysis of magnetic hybrid Nano-fluid natural convective flow in an adjusted porous trapezoidal enclosure. *Journal of Magnetism and Magnetic Materials*, 564, 170142. doi: 10.1016/j.jmmm.2022.170142
- [53] Rostami, S., Aghakhani, S., Hajatzadeh Pordanjani, A., Afrand, M., Cheraghian, G., Oztop, H.F., & Shadloo, M.S. (2020). A review on the control parameters of natural convection in different shaped cavities with and without nanofluid. *Processes*, 8(9), 1011. doi: 10.3390/pr8091011
- [54] Basak, T., Roy, S., & Thirumalesha, C. (2007). Finite element analysis of natural convection in a triangular enclosure: effects of various thermal boundary conditions. *Chemical Engineering Science*, 62(9), 2623–2640. doi: 10.1016/j.ces.2007.01.053
- [55] Siddiki, M.N.A.A., Islam, S., Ahmmed, M.U., & Molla, M.M. (2024). Numerical simulation of a non-Newtonian nanofluid on mixed convection in a rectangular enclosure with two rotating cylinders. *International Journal of Ambient Energy*, 45(1), 2332525. doi: 10.1080/01430750.2024.2332525
- [56] Sivakumar, V., Sivasankaran, S., Prakash, P., & Lee, J. (2010).
 Effect of heating location and size on mixed convection in lid-

- driven cavities. *Computers & Mathematics with Applications*, 59(9), 3053–3065. doi: 10.1016/j.camwa.2010.02.025
- [57] Montgomery, D.C. (2017). *Design and analysis of experiments*. (9th ed.) John Wiley & Sons.
- [58] Box, G.E., & Wilson, K.B. (1992). On the experimental attainment of optimum conditions. In *Breakthroughs in statistics:*
- methodology and distribution (pp. 270–310). Springer New York. doi: 10.1007/978-1-4612-4380-9_23
- [59] Campolongo, F., & Braddock, R. (1999). The use of graph theory in the sensitivity analysis of the model output: a second order screening method. *Reliability Engineering & System Safety*, 64(1), 1–12. doi: 10.1016/S0951-8320(98)00008-8